IDENTIFICATION OF PILOT CONTROL BEHAVIOR DURING POSSIBLE ROTORCRAFT PILOT COUPLING EVENTS

Deniz Yilmaz[1], Marilena Pavel[2]
Delft University of Technology (Netherlands)

d.yilmaz@tudelft.nl,
m.d.pavel@tudelft.nl

Michael Jones[3], Mike Jump[4], Linghai Lu[5]
The University of Liverpool (United Kingdom)

michael.jones@liverpool.ac.uk,
mjump1@liverpool.ac.uk,
Linghai@liverpool.ac.uk

Abstract

The goal of the present paper is to understand pilot control behaviour during "possible" Rotorcraft Pilot Coupling (RPC) events. Two identification experiments were conducted in two simulation facilities with four current helicopter test pilots. The experiments used a single loop roll disturbance-rejection hover task, with a time delay applied in the pilots control path during the simulation in order to trigger a RPC event. Two linear identification methods in frequency and time domain, Fourier Coefficients and Maximum Likelihood Estimation respectively, were applied as a part of the cybernetics approach to Phase I (without RPC) and Phase II (with possible RPC) partition of each simulation run. Real-Time Oscillation VERifier was used to determine whether RPCs occurred during Phase II of each simulation run. Pilots were found to consistently adapt their behaviour to counter the applied time delay in Phase II, in both simulation facilities. Proposed pilot model and corresponding model parameter deviations to cope with triggered RPC are presented within this paper. Pilot control behaviour adaptations during possible RPC events were mainly observed during the low frequency compensation partition of the wide-frequency manual control task.

NOTATION

ϕ	Roll angle, rad
L_p	Roll damping, 1/s
$B_{\theta_{1c}}$	Lateral Control Matrix element, 1/s^2
θ_{1c}	Lateral swash plate input, rad
K_{gear}	Lateral cyclic Gearing, rad/(% input)
δ_{lat}	Lateral cyclic input, %
δ_{lat_sim}	Simulated lateral cyclic input, %
f_d	Disturbance forcing function, rad
ϕ_{trim}	Trim roll angle, 0 rad
e_ϕ	Roll angle error, rad
$f_{d,t}(t)$	Disturbance forcing function, rad
$N_{d,t}$	Number of sinusoid frequencies in disturbance forcing function
K^*	Amplitude scaling factor
$A_{d,t}(k)$	Amplitude distribution of disturbance forcing function, rad
$\omega_{d,t}(k)$	Sinusoid frequencies distribution of disturbance forcing function, rad/s
$\phi_{d,t}(k)$	Phase distribution of disturbance forcing function
ω_m	Measurement time frequency, rad/s
$e^{-j\omega\alpha}$	Low frequency lag phase correction
ω_b	Break frequency, rad/s
$H_p(j\omega)$	Precision pilot model
T_L	Lead time constant, s
T_I	Lag time constant, s
K_p	Pilot gain, -
T_N	Neuromuscular lag, s
ω_{nm}	Neuromuscular frequency, rad/s
ζ_{nm}	Neuromuscular damping, rad/s
τ	Pilot time delay, s
T_K	Low frequency lead time constant, s
T'_K	Low frequency lag time constant, s
T_m	Measurement time, s
ω_m	Measurement frequency, rad/s

ACRONYMS

APC	Aircraft Pilot Coupling
A/RPC	Aircraft/Rotorcraft Pilot Coupling
ADS	Aeronautical Design Standard
AG	Action Group
ARISTOTEL	Aircraft and Rotorcraft Pilot Couplings: Tools and Techniques for Alleviation and Detection
CNS	Central Nervous System
EC	European Commission
FC	Fourier Coefficient

Paper presented at the 38th European Rotorcraft Forum, Amsterdam, The Netherlands, September 4 – 7, 2012.

[1] PhD Student, Delft University of Technology, Aerospace Engineering Department,Netherlands
[2] Assoc. Prof. Dr, Delft University of Technology, Aerospace Engineering Department,Netherlands
[3] PhD Student, University of Liverpool, School of Engineering,UK
[4] Lecturer, University of Liverpool, School of Engineering,UK
[5] Research Assistant, University of Liverpool, School of Engineering,UK

FCS	Flight Control System
FFT	Fast Fourier Transformation
FP7	7th Framework Programme
FT	Flight Test
FBW	Fly-by-Wire
GARTEUR	Group for Aeronautical Research and Technology in Europe
HFR	HELIFLIGHT-R
HQR	Handling Qualities Rating
LTI	Linear Time Invariant
MLE	Maximum Likelihood Estimation
MTE	Mission Task Element
ONERA	Office National d'Etudes et de Recherches Aerospatiales (The French Aerospace Laboratory)
PAO	Pilot Assisted Oscillations
PIO	Pilot-Induced Oscillations
PIOR	Pilot-Induced Oscillations Susceptibility Rating
PLE	Position Limiting Element
PVS	Pilot-Vehicle System
RB	Rigid Body
RLE	Rate Limiting Element
RMS	Root Mean Square
ROVER	Real-Time Oscillation VERifer
RPC	Rotorcraft Pilot Coupling
SIMONA	Simulation, Motion and Navigation
SOS	Sum of Sinusoids
SRS	SIMONA Research Simulator
STD	Standard Deviation
TUD	Delft University of Technology
UoL	University of Liverpool
VAF	Variance Accounted For

1. INTRODUCTION

Rotorcraft Pilot Couplings (RPCs) – including "pilot induced/assisted oscillations" (PIO/PAO)- refer to inadvertent, sustained aircraft oscillations which are a consequence of an abnormal joint enterprise between the aircraft and the pilot [2]. In other words, RPC events are unexpected and potentially catastrophic instabilities, the convergent RPCs are manifested as limit cycle oscillations that arise from pilot effort to control the aircraft. RPCs are typically triggered by a "mismatch" between the pilot and the vehicle dynamics. This mismatch manifests active PIOs and/or passive PAO's participation of the pilot in the control loop [2]. Despite decades of work to develop methods for their prevention, unfavourable aircraft/rotorcraft pilot couplings (A/RPCs) continue to occur. To extend the understanding of RPCs, GARTEUR HC AG-16 was formed and was composed of a number of European universities and industry partners in 2005 [11]. In 2010, the European Commission (EC) launched, under the umbrella of the 7th Framework Programme (FP7), the ARISTOTEL project [9] (Aircraft and Rotorcraft Pilot Couplings – Tools and Techniques for Alleviation and Detection) to extend the gathered knowledge from GARTEUR HC AG-16. The aim of ARISTOTEL project is to advance the state-of-the-art in A/RPC prediction and suppression. With duration of 3 years and involving partners from across Europe, the ARISTOTEL project[1] objectives are to improve the physical understanding of present and future A/RPCs and to define criteria to quantify an aircraft's susceptibility to A/RPC.

According to the degree of non-linearity of the oscillation of the Pilot-Vehicle System (PVS), RPC are divided in four main categories [2]: Category I RPC's are essentially linear and are a direct consequence of system time delays, or phase lags in the vehicle/control path dynamics. Category II A/RPC's are quasi-linear events and are triggered by the nonlinear rate and/or position limiting elements (RLEs and/or PLEs). Category III A/RPC's are essentially non-linear PVS oscillations with transitions in command type of the Flight Control System (FCS) that cause a pilot mental mismatch. Category IV A/RPC's are oscillations due to the coupling of elastic structural modes (Aeroelastic) and the pilot or due to biodynamical couplings.

Throughout the GARTEUR HC AG-16 project, application of time delays to the control paths of the pilot control inceptors and rate limiting on the main rotor swash plate actuators resulted in successful triggering of RPCs during simulation test campaign trials [11], supported by subjective pilot handling qualities ratings (HQRs) and PIO ratings (PIORs). The study of this paper also uses the application of time delays (300ms) on the pilot cyclic as a trigger for 'possible' RPC situations. This is equivalent to triggering a Cat. I RPC event.

For RPCs to occur, three key elements are required: the vehicle, the pilot and the trigger. In a broad terms, a vehicle with poor handling qualities [1], a pilot with out-of phase tight control strategy[34], and an external or internal triggering factor[2] (e.g. Fly-by-wire (FBW) software node change or actuator rate limiting) together form a higher potential for RPC than a rotorcraft holding good handling qualities with a pilot who is familiar to RPC events with good RPC suppressing skills such as breaking the loop instead of tightening the control to override the triggered RPC.

Starting from the Wright Brothers first flight, pilot vehicle system (PVS) closed loop instabilities, and one step further PIO's (namely A/RPC's), have been considered an important research area, directly affecting the safety features of the aircraft and the crew. It is worth mentioning that A/RPC studies (e.g. [2],[11],[12],[13]) have revealed that it is not just the pilot or the vehicle that is the 'guilty element' in an RPC event. It has been emphasized that it is the coupling and interaction of both elements that cause the instability. The study reported in this paper aims

to determine *the pilot's* role in the instability, in the presence of vehicle dynamics and a trigger situation known to cause RPC events.
This paper describes a set of experiments conducted in simulation facilities both at the Delft University of Technology (TUD), Netherlands and the University of Liverpool (UoL), UK. The scope of this study was to understand the role of the pilot control strategy during a time delay triggered 'possible' RPC event for a hover stabilization task of a Bo105 rotorcraft simulation model within a designed disturbance rejection task. The underlined elements of the statement above were included in a scenario within a controlled simulator environment, and an identification methodology was applied to investigate the pilot model during a "possible" RPC task.

In 2000, Mitchell[34] published a study to identify the pilot in PIO's, which were recorded during fixed wing HAVE PIO flight tests [40] and ground simulations [39]. Pilot control strategies were categorized as synchronous and compensatory, depending on the pilot's compensation effort and ultimately the task. This study was proposed to understand the characteristics of the pilot immediately before and after the PIO, to enhance the determination of RPC suppression methods. Especially, sum of sinusoids (SOS) tracking data provided a good basis to investigate PIO frequency per pilot, which was calculated by peak to peak values of vehicle body rate responses. Considering the fact that the ground simulation in ref. [34] was originally aimed to identify the pilot for different vehicle configurations (not focused on APCs), the measurement data were not fully compatible with identification of a pilot behaviour for PIOs. However, extracted data concluded that pilots showed different tendencies to detect and respond to PIO conditions (PIO frequency).

Multi modal human identification methods have been used in many fields of human-operator controlled systems and have recently received much interest in the specialist literature [15]. This wide spectrum of human identification research also includes rotorcraft pilot identifications. This technique can be a challenge for rotorcraft applications due to the inherent instability of the controlled element and multiple loop coupled pilot control activities. Nieuwenhuizen et. al. [3] investigated the identification of helicopter pilots for a roll and lateral displacement (two degree of freedom) model, during a target tracking and disturbance-rejection manual task. The scope of the experiment was to investigate the motion feedback effects on perception and control strategy of the pilot model for the designed task. In addition to the common approach of considering the rotorcraft pilot models as Linear Time Invariant (LTI) systems, there is a growing interest in time varying human operator identification. Recently (2011), Zaal and Sweet [6] presented research on a time variant pilot model estimation by using offline simulation models with/without remnant. The simulations showed that the Wavelet method, which has the capability to capture time and frequency resolutions, is prone to inaccuracy depending on the remnant level, whereas windowed Maximum Likelihood Estimation (MLE) shows better accuracy. However, this brings with it the penalty of missing fast changes in pilot control behaviour. In 2011 Klyde et al [7] used a Wavelet method to characterize the rotorcraft pilot-vehicle interactions for added dynamics (lead/lag second order dipole pairs) throughout a piloted precision hover task with uncoupled OH-6A dynamics. The Wavelet method successfully showed the transition phases of pilot activity and vehicle responses as the dynamics varied. Finally, a study also published in 2011, concentrated on the adaptation of human pilot dynamics in the control of time-varying systems (added first order low pass filter) for a multi-loop uncoupled rotorcraft model [8]. The study focused on bode-representations of open-loop responses of human-vehicle system, instead of identified pilot parameters.
.
This paper is structured as follows: First, the methodology of the pilot model identification procedures is discussed. Second, the experimental setup is discussed. Third, the results are given. Finally, conclusions are drawn and recommendations are made.

2. METHODOLOGY

A disturbance rejection manual control task was designed to control a single axis (roll degree of freedom) Bo105 simulation model. The schematic representation of this single compensatory control loop is shown in Figure 1.

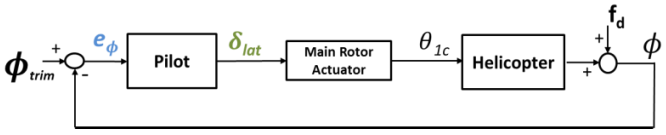

Figure 1 .*The closed-loop manual control task with forcing function f_d, roll angle $\boldsymbol{\phi}$, 0 trim bank angle $\boldsymbol{\phi_{trim}}$, displayed roll angle error $\boldsymbol{e_\phi}$, pilot lateral cyclic input $\boldsymbol{\delta_{lat}}$, and main rotor swash plate deflection $\boldsymbol{\theta_{1c}}$.*

The following Sections describe the components of the closed loop control task and the identification methods used.

2.1 Disturbance Forcing Function (f_d)

To be able to identify the pilot control behaviour for the designed task, a disturbance forcing

function (f_d) was designed to have sufficient frequency content to excite the pilot response bandwidth of interest, which contains low frequency content for active pilot control and high frequency content to stimulate neuromuscular adaptation. In agreement with McRuer's description [1], the disturbance forcing function is composed of a sum of 10 ($N_{d,t}$) sinusoids:

$$f_{\mathrm{d,t}}(\mathrm{t}) = \sum_{k=1}^{N_{d,t}} K^{*} A_{\mathrm{d,t}}(\mathrm{k}) \sin[\omega_{\mathrm{d,t}}(\mathrm{k})\mathrm{t} + \phi_{\mathrm{d,t}}(\mathrm{k})] \quad (1)$$

The amplitude, $A_{\mathrm{d,t}}(\mathrm{k})$, frequency $\omega_{\mathrm{d,t}}(\mathrm{k})$ and phase $\phi_{\mathrm{d,t}}$ distribution of the initial SOS disturbance signal is listed in Table 1. The amplitude distribution is shown in Figure 2.

Disturbance Signal (f_d) Design				
k_d	**n_d**	**ω_d**, rad/s	**A_d**, rad	**ϕ_d** ,rad
1	5	0.3835	0.01	-0.269
2	11	0.8437	0.01	4.016
3	23	1.7641	0.01	-0.806
4	37	2.8379	0.005	4.938
5	51	3.9117	0.005	5.442
6	71	5.4456	0.005	2.274
7	101	7.7466	0.005	1.636
8	137	10.5078	0.005	2.973
9	177	13.5757	0.005	3.429
10	126	17.3340	0.005	3.486

Table 1. *Experiment disturbance forcing function design settings.*

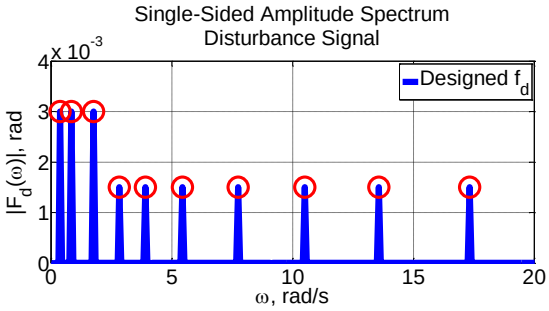

Figure 2 .*Disturbance forcing function amplitude distributions*

From a design point of view, there is a trade-off between having powerful high and low frequency content of the disturbance; high power in low frequency leads to a predictable disturbance signal for the pilot to track, whereas high power in high frequency results in a very difficult to track chaotic signal which leads the pilot to believe they have no control. To account for this, a scaling factor was introduced to set the overall designed forcing function to an unpredictable disturbance, with noticeable high frequency content. This tuning was performed with two helicopter pilots and finally the whole bandwidth scaling factor (K^{*} in Eq. (1)) was set to 0.3 by conducting shakedown tests prior to the identification experiment. Thus, a hard to predict disturbance signal was obtained which did not require excessive pilot control but with sufficient high frequency content. The resultant time trace of the applied disturbance forcing function is shown in Figure 3, with the marker showing the start of the forcing function repetition basis measurement time ($T_m = 81.92\ s$).

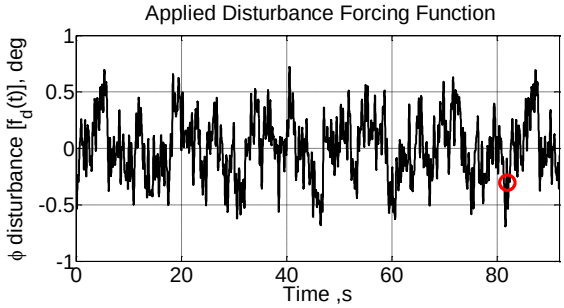

Figure 3 .*Disturbance forcing function time trace.*

The sinusoid frequencies of the disturbance signal are approximately logarithmically spaced from 0.3 to 18 rad/s, to allow pilot identification methods to be used by spectral methods [14]. The measurement time was set to 81.92 seconds, which contains the highest power-of-two data points and these sinusoid frequencies are integer multiples of the measurement time frequency, $\omega_{\mathrm{m}} = 2\pi/T_m = 0.0767$ rad/s. The repetition numbers of the sinusoidal frequencies (n_d) and the random phase distribution (ϕ_d) are shown in Table 1. The signal's phase distribution was checked for possible undesirable clustering around some frequencies and the resultant signal, shown in Figure 3, was decided to be within the pilot control margin.

2.2 Controlled element (The Helicopter Model and Main Rotor Actuator Model)

A representative 1-dof Bo105 was extracted from a linearized analytical rotorcraft model, which was developed specifically for use in the first ARISTOTEL Rigid Body (RB) test campaign [33]. The characteristics of the uncoupled roll simulation model are essentially defined by the roll subsidence mode of the rotorcraft (in the hover condition). This mode is also driven by the roll damping (Lp) of the helicopter, which has been verified with other ARISTOTEL partner simulation models], shown in Figure 4, and the literature [26].

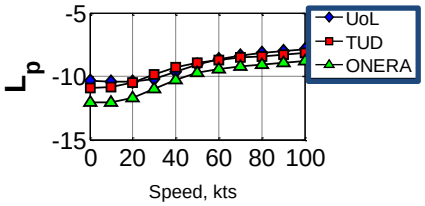

Figure 4. *Rolling damping, Lp, of simulation models for increasing forward velocities*.

The equation of motion for the simplified linear Bo105, the controlled element, can be expressed as;

$$\ddot{\phi} = L_p\dot{\phi} + B_{\theta_{1c}}\theta_{1c} \quad (2)$$

$$\theta_{1c} = K_{gear}\delta_{lat} \quad (3)$$

where ϕ is the roll angle, L_p is the roll damping, $B_{\theta_{1c}}$ is the control matrix element of lateral swash-plate input and θ_{1c} is the commanded swash-plate angle. Equation (3) represents the direct mechanical gearing (K_{gear}) between pilot cyclic input (δ_{lat}) to swash-plate angle deflection (θ_{1c}). Here, for simplicity of analysis, no actuator model was introduced (despite its use in the original model). Instead, one-to-one gearing from cyclic input to actuator deflection was utilised. Therefore, any commanded actuator deflection angle was directly achieved without any additionally incurred time delay or rate limiting. Figure 5 shows the Bode diagram for the system described in Eqns. (2) and (3).

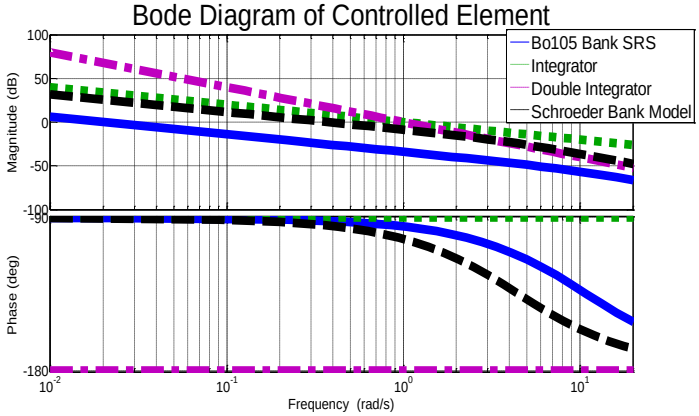

Figure 5. *Bode diagram of Bo 105 bank model used in the experiment, an integrator, a double integrator and Schroeder's roll model*

It can be seen from the bode comparison Figure 5 that the controlled element, the model of the Bo105 model in this study, behaves like a unity integrator for low and moderate (0.3 to 11 rad/s in this study) human pilot control frequencies and switches to double integrator behavior for the high frequency portion (above 11 rad/s). The break frequency of the model (11 rad/s) and the roll-lateral coordinated model [4] (5.5 rad/s) is also shown in Figure 5, indicated by the later convergence to magnitude and phase (-180 degrees) of double integrator from the single integrator (-90 degrees).

2.3 Identification Methods

It was assumed that in the experiment, pilots achieved a linear control strategy without time dependency, except the transition part just after when the time delay in the control path was applied. In order to capture the behavior of the pilot, two LTI identification methods were used in the experiment set. The 1st method was the non-parametric frequency domain Fourier Coefficients (FC) method followed by a model parameter optimization. The 2nd identification technique was the parametric time domain Maximum Likelihood Estimation method.

2.3.1 Fourier Coefficients (FC) Method

The FC method uses the Fast Fourier Transformation (FFT) of input to the pilot models ($\boldsymbol{e_\phi}$) and the corresponding control input of the pilot ($\boldsymbol{\delta_{lat}}$), to extract the frequency content at the enriched forcing function frequencies. Instead of describing the pilot model structure, this frequency domain method provides the non-parameterised, analytic pilot model response describing functions [14,29].
Furthermore, an embedded optimization tool (lsqnonlin) in MATLAB® was used to minimize the frequency response error between the measured FC model and the proposed pilot model frequency response, whilst also using pilot parameters as optimization variables. This tool solves non-linear least squares problems with either trust region reflective or Levenberg-Marquardt algorithms [19]. The trust region reflective section of the algorithm is a bounded parameter optimization, which requires low and high bounds of the parameter interval.

From here, the term "FC identification" used in this paper refers to following two-step pilot modeling technique; **1.** FC of measurement data, **2.** Optimisation of pilot parameters to achieve minimum frequency model error to fit the measurement data.

2.3.2 Maximum Likelihood Estimation (MLE) Method

The MLE method is a time domain identification technique where the Jacobian matrices of the proposed pilot model and the corresponding Fisher information matrix are used. With adaptive line search vectors, likelihoods of optimisation iteration steps are obtained for the proposed pilot model in the algorithm. The cost function of the gradient based Gauss Newton optimisation method is defined by minimising the error between time domain response of the proposed pilot model and the time domain measurement [20,43,44].

Briefly, the essence of MLE is to find the joint probability function for the "predicted" error, which is the error between the actual measurement data and the result of the model. More specifically, the required probability function should make the parameter estimate "most likely" by maximizing the likelihood function, which is presented in Eq.(4) [20,43,44].

(4) $$L(\theta) = f(\varepsilon_1, \varepsilon_2, \dots, \varepsilon_N; \theta)$$

where L is the likelihood function, ε is the predicted error, θ is the parameter vector and N is the sample size of the measurement data.

The Gauss Newton optimization routine aims to find the parameter vector (Eq.(5)[37]) which maximizes the likelihood function Eq.(4) ;

(5) $$\theta^* = \arg\max_\theta \ln L(\theta) = arg\ \min_\theta \frac{1}{2\sigma_\varepsilon^2}\sum_{i=1}^{N} \varepsilon_i^2$$

where θ^* is the parameter set which results in maximum likelihood function, $\sigma_\varepsilon$is the error variance, and ε is the predicted error. One of the common issues of MLE is localizing around a local minimum, instead of the global one. One practical remedy is to chance the initial conditions and assuming a global minimum if all the selected initial conditions converges to the same minimum[37]. Another remedy (computationally expensive) is using Genetic Algorithm to automize and optimize the selection of initial condition[30].
More detailed information on MLE identification technique can be found in Ref [20,43,44].
In this study, initial conditions were obtained from FC identification results, and the internal optimization routine is the convex Gauss Newton. Considering the importance of the initial conditions in such a gradient based optimization, good time domain model fit values of FC results lead to the assumption that the global minima could be in the vicinity of these parameter set.

2.4 Pilot models

Stemming from McRuer's crossover model [1], various pilot modelling structures have been developed in the literature, as summarized in Refs. [23,27]. Control strategy models have focused on pilot equalisation techniques to perform the task, whereas structural models aim to model pilot's structural components with detailed muscle-neuron, partial central nervous system (CNS), and vestibular system organs (i.e. otoliths, etc.)

In this paper, the aim is to identify the pilot through the use of McRuer's Precision Model[1,17], a modified version of the extended crossover model that covers a wider frequency range (0.1 rad/s up to 20-30 rad/s depending on the neuromuscular resonance):

$$H_p(j\omega) = \overbrace{K_p\left(\frac{T_L j\omega + 1}{T_I j\omega + 1}\right)}^{\text{pilot equalization}} \overbrace{\left(\frac{T_K j\omega + 1}{T'_K j\omega + 1}\right)}^{\text{low-freq lag lead}} \times \underbrace{\left[\frac{{\omega_{nm}}^2}{(T_N j\omega + 1)([jw]^2 + 2\zeta_{nm} jw + {\omega_{nm}}^2)}\right]}_{\text{neuromuscular dynamics}} \underbrace{e^{-j\omega\tau}}_{\text{pilot delay}} \quad (6)$$

The Precision Model (described by Eq(6) features a general pilot equalisation term with lead and lag (T_L and T_I respectively), a pilot visual gain (K_p), a neuromuscular model with lag (T_N), neuromuscular natural frequency (ω_{nm}) and damping(ζ_{nm}), a pilot time delay (τ), and low frequency equalization lead-lag term (T_K and T'_K respectively).

The reader should note that the pilot equalization part of the model is generic, depending on the controlled element dynamics. In the results Section of this paper, the pilot equalisation for the experiment controlled element, Figure 5, will be taken into consideration and the required pilot model structure will be discussed depending on the measurement data and the controlled element dynamics.

3. APARATUS AND EXPERIMENT SETUP

3.1 Flight Simulator Facilities

Two simulation facilities were used in this experiment set; SIMONA (SRS)[24] at TUD, and HELIFLIGHT-R(HFR)[18] at UoL, shown in Figure 6.

(a) (b)

Figure 6. a) *SIMONA research simulator TU Delft, Netherlands, b) Heliflight-R research simulator[25] Liverpool University, UK.*

The compensatory model is based on the assumption that pilot responds to the error that they perceive. Therefore, the visual environment projector displays were turned off to prevent the pilots using any visual cues. It also mitigated against the possibility of pilots introducing a feed-forward control strategy [28]. Since it is crucial to respond to the perceived error of roll angle in this compensatory setup, the scale of displayed error was considered to be important. Ref. [22] showed the positive effect of indicator display size on roll axis tracking task performance. In the current experimental setup, the perceived errors were displayed through scaled up attitude

indicators from the original console displays in both simulators, shown in Figure 7 with dimensions of displays.

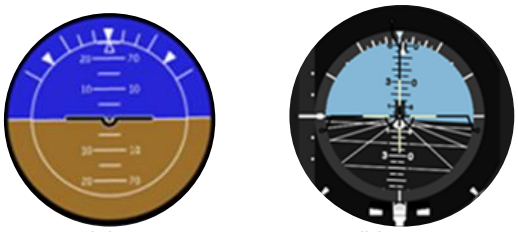

(a) (b)

Figure 7 . *a) The scaled up attitude indicator in SIMONA. Indicator outer and inner ring diameters are 13 cm, 9.5 cm respectively. The display distance to eye design point of the pilot seat is approximately 85 cm. b) The scaled up attitude indicator in HFR. Indicator outer and inner ring diameters are 15 cm, 13 cm respectively. The display distance to eye design point of the pilot seat is approximately 90 cm.*

The motion systems of both simulators were switched off to prevent pilot vestibular feedback. Finally, a pure compensatory visual model was achieved. Although the cyclic controllers of simulators are not identical, the control feel system settings were matched as far as possible within the existing software's capabilities. Both cyclic lateral force gradients were set to approximately 4N/deg, and a small breakout force was maintained to preserve the continuity of the simulator test campaign, as the pilots used were already familiar with the simulator configurations. Considering the fact that LTI linear model identification methods require consistent linear responses from the pilot, it was assumed that the nonlinearities arising from control inceptor dynamics were not dominant and they could be considered to be included in the pilot remnant.

This experimental task setup resembles a scenario whereby a high roll turbulence in zero visibility (e.g. in cloud) is being experienced that forces pilot to use his instrument flight skills. However, it must be noted that the lack of motion cues, and isolated and uncoordinated single axis control/response makes the SOS task noticeably 'unrealistic'' for pilots. Similar identification trials have also reported the lack of realism in such setups [30,34,38]. Although this lack of realism may be seen as a drawback of the investigation, it is assumed that using simulator helicopter cyclic inceptors, locating the pilots in the actual simulator environments (where pilots practiced full capability ADS-33 Mission Task Elements(MTEs)) and actual attitude indicators (unlike artificial roll error displays) would achieve a higher level of realism when compared to a laboratory tracking task setup.

3.2 Experiment Setup

3.2.1 Measurement Settings

As mentioned in Section 2.1, the measurement time for the pilot identification was 81.92 seconds. An additional 10 seconds was introduced to account for pilot adaptation to the task and translate into linear control behaviour; 8 seconds of fade in and 2 seconds of fade out. Two separate sets of identification data were gathered; 'training' and 'full' runs. The two sets of tests are as follows;

- Training: 4 training runs per pilot were generated for 91.92 seconds. The fade in and fade out parts of the measurement data were omitted and frequency domain matching was performed for $T_m = 81.92\ s$.
- Full run: Four runs of full length measurement were performed per pilot. A full run consist of a continuous 183.84 seconds, which is composed of a no time delay partition for the first 91.92 seconds and a time delay applied second portion of 91.92 seconds duration. These two phases are termed as Phase I, standing for "no time delay applied" first partition, and Phase II standing for the "time delay applied" second partition. For clarity, Figure 8 shows the full run measurement time axis and corresponding parts and identification intervals with fade in and fade out time segments.

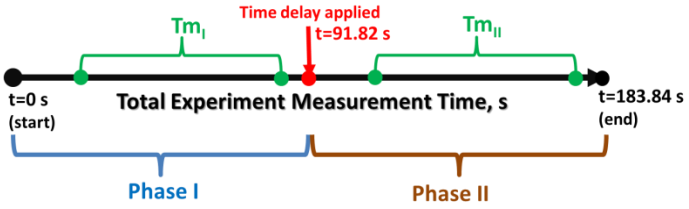

Figure 8. *A sample sketch of a full run time axis showing the Phase I and Phase II partitions, applied time delay activation time, and measurement times (T_{mI} and T_{mII}) that were used for identification methods.*

Here, it is important to mention the transition measurement time between Phase I and Phase II.

McRuer [10] concludes that the transition dynamics of the pilot from one controlled element to an altered one requires time to adapt. This is called the *Post-Transition Retention* [10].Throughout the transition phase, the pilot still believes that they are controlling the vehicle operated prior to the change of control element dynamics. Following this period, the pilot adapts to the altered control element dynamics and finally compensates for the final control element. In this experiment set, it was assumed that the

fade out time of Phase I in addition to the fade in time of Phase II (which are 2s + 8s respectively) provided sufficient time for the pilot to adapt his linear control strategy to the altered controlled element dynamics, namely the time delay applied during Phase II.

3.2.2 Participants

Four experienced helicopter pilots participated in both simulator experiments. Each pilot had a short familiarisation run which did not include the external disturbance, allowing them to acclimatise to the response of the controlled element (roll model). After the familiarisation run, 4 training runs were performed followed by 4 'full' runs per pilot. Between all runs, a short break was provided to keep the pilots rested. Here, it must be noted that the task of focusing the bank error on the attitude indicator in a dark simulator cabin requires extensive attention from each pilot. As pilots were not provided with any post run statistical performance feedback (like Root Mean Square (RMS) of error), they were required to subjectively adjust their performance level. This situation was also a matter of overall task handicap which implies the lack of detecting pilot back-off from the task (when the pilot ignores the displayed error and reduces his responses). . Recommendations Section will extend the discussion of this matter with proposed remedies.

Table 2 lists the experience of the pilots who participated in the identification experiment set.

Pilot	Current Job	Rotary-wing hours	Fixed-wing hours	Sim hours
A	Senior Captain for Commercial Airline	3000	11000	5000
B	Senior First Officer for Commercial Airline/British Royal Navy	7800	8000	1300
C	Royal Netherlands Airforce – Chinook Test Pilot	1500	200	230
D	Royal Netherlands Airforce – Apache Test Pilot	2000	150	400

Table 2. *Pilot experiences extracted from Ref.* [33]

4. RESULTS

The results of the experiment will be explained in this Section. First the overall frequency content of the measurement data will be presented to understand the general tendency of pilot adaptations to the task and simulator environments.
This subsection is essentially the first part of the FC identification method.
The second subsection introduces the pilot model structure that describes the pilot compensation and model fit. The justification and parameterization of the selected pilot model will be reported in this subsection with adaptation to both FC and MLE identification methods. The third subsection will show the pilot model parameter changes for the recorded measurement data with various comparison bases.

4.1 Frequency content of measurement data

Before applying any pilot model estimation, the frequency content of the measurement data should be checked to verify the trace of rich content on the disturbance frequencies in the pilot response and detection of possible low signal-to-noise ratios.

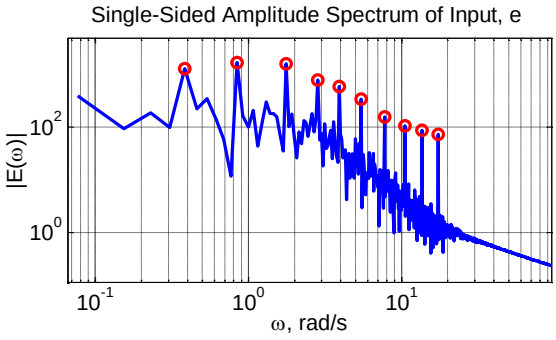

Figure 9. *Single sided amplitude spectrum of pilot perceived bank angle error, e (the input to pilot model, indicated as e_ϕ in Figure 1) and pilot control, u (the output to pilot model, indicated as δ_{lat} in Figure 1) of a sample run, where the designed disturbance function frequencies are marked with circles.*

Figure 9 shows the displayed visual roll angle error. Fig.9–a contains the rich content of the disturbance function, which is expected when the task design allows direct implementation of disturbance to state output of the controlled element, like in this experiment. More important is the output of the pilot (Figure 9 –b) as this may include high frequency noise in the measurement data and merge or lump nonlinearities into high frequency content of his output, which combines with nonlinearities of the

inceptor. Large power content in the high frequency bands of the disturbance function (see Figure 2) resulted in noticeable rich high frequency content, which is an indication that the pilot responded to the frequencies contained within the disturbance forcing function. Even though it is beneficial to have high signal to noise ratio, it may end up with a very hard task for pilots to complete, or occurrence of pilot crossover regression to bypass the high frequency content. Nevertheless, the clear peaks of high power in both input and output of the pilot model set a good identification quality basis.

Further investigation of the frequency content of the measurement data shows pilot control adaptations for the training, Phase I (no time delay) and Phase II (with time delay) partitions of the experiment runs.

As an example, measured responses of pilot B in SIMONA for training, Phase I and Phase II partitions are shown in Figure 10.

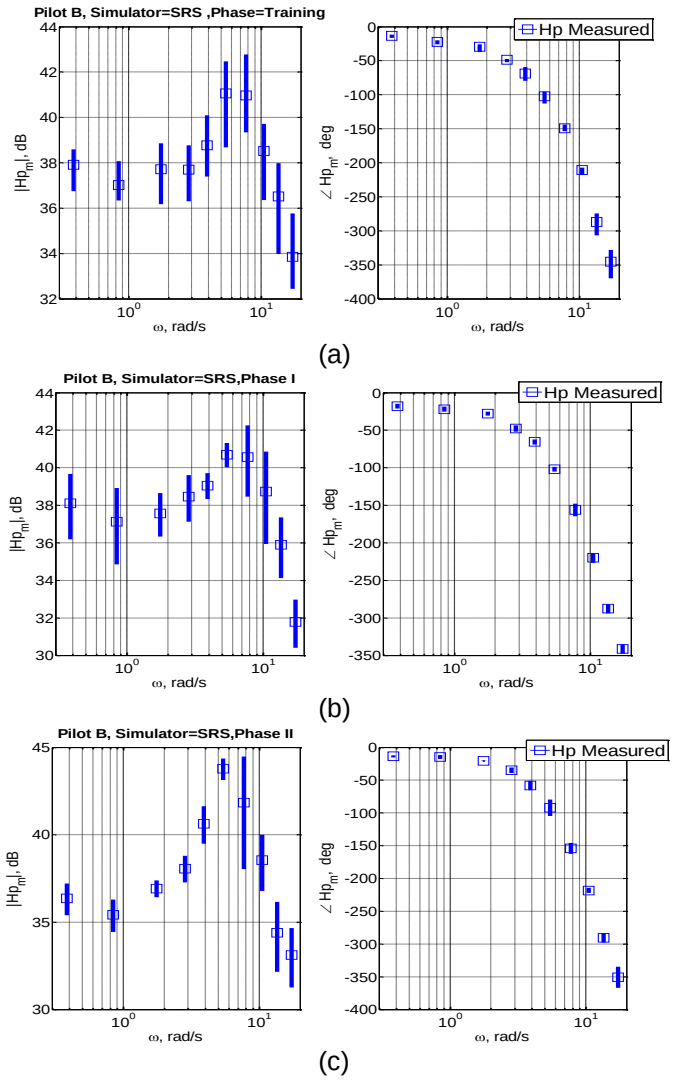

Figure 10. *Measured frequency response of pilot B (Hp Measured), in SRS simulator for training (a), Phase I (b) and Phase II (c), with mean of each frequency point (square markers) with corresponding standard deviation(std) bars for four runs of each partition.*

It is observed from Figure 10 that the frequency content of the training phase has more sparse data in the magnitude plot than the phase of the pilot response The Phase II portion of the test showed a consistent response of the pilot at low frequencies and more varying responses around neuromuscular natural frequencies [1], during different runs. Furthermore, the variance in magnitude is more noticeable than the variance of phase, regardless of the task phase. Similar trends are also observed for the other pilots.

From another point of view, Figure 11 shows the difference of mean values of frequency responses for each task partition for tests performed in both simulators.

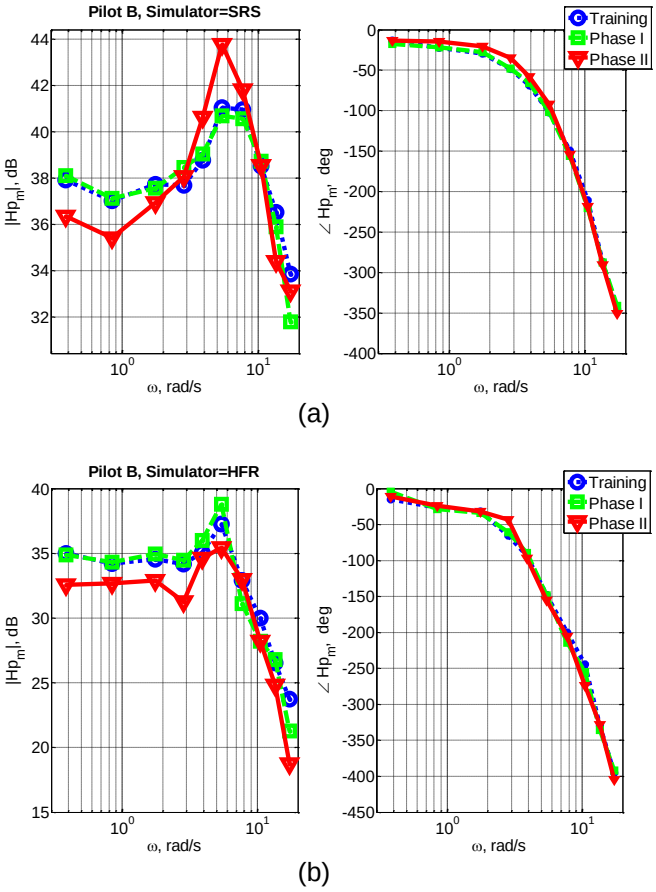

Figure 11. *Measured mean frequency response of pilot B in SRS (a) and HFR (b) simulators for training, Phase I and Phase II partitions of the experiment runs.*

Figure 11 shows that pilot B showed good training skills for the task, indicated by a very close response between training and Phase I, which are essentially the same disturbance and no-time delay portions of the experiment. Moreover, the pilot adaptation to “possible” RPC scenario is also apparent with the distinct frequency response for magnitude (a low frequency drop) and partially in phase (higher lead, or less pilot time delay up to 6-7 rad/s). All

pilots showed a consistent pilot control strategy adaptation to the degraded helicopter model, regardless of the simulator. Before starting any pilot model fitting to the measurement data, this non parametric identification (which is essentially the first step of the FC method) already indicates a comprehensive pilot adaptation to the RPC prone task.

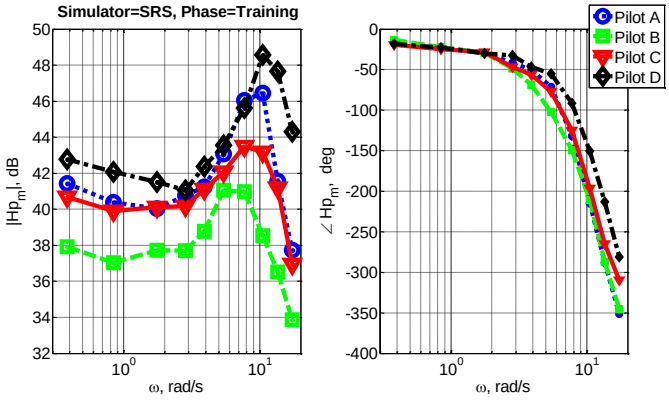

(a)

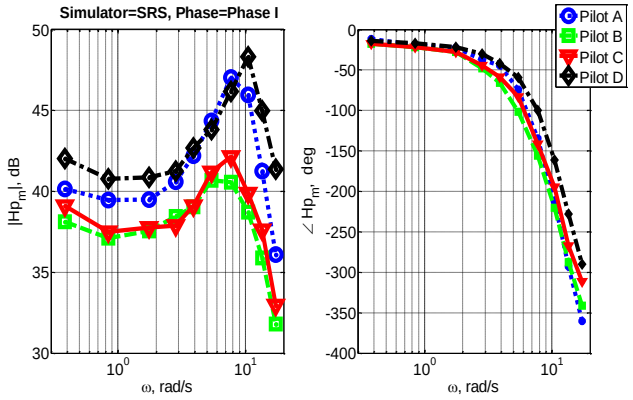

(b)

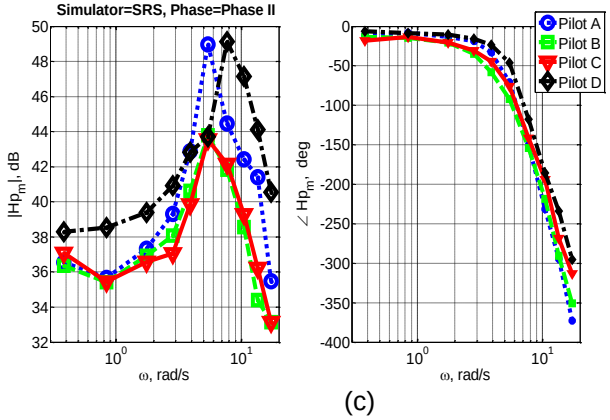

(c)

Figure 12 *Measured pilot frequency responses for training (a), Phase I (b) and Phase II (c) of the task for four pilots in SRS simulator*.

Figure 12 shows the difference between all pilots when completing the task in SRS. During the training sessions (Figure 12-a), Pilot A and Pilot C showed similar performance in both magnitude and phase. The gain offset (the vertical shift in magnitude) also shows pilot adaptation differences, containing the neuromuscular activation. Phase I (Figure 12-b), which is essentially the same as the training phase, shows that Pilot C lowers his gain and coincides with pilot B, while pilot A and D keep almost the same training frequency response. This gives a hint about the level of training, and the achieved consistency within the same task. Phase II (Figure 12-b), which contains the "possible" RPC condition, shows an interesting adaptation among pilots; with the exception of Pilot D, all pilots matched almost the same low frequency magnitude response with different neuromuscular frequency and damping. The reader's attention is drawn to the response of Pilot A, who showed signs of a significant under-damped neuromuscular activation when compared to Phase I results. Furthermore, Pilot D showed a lower phase lag response at the lowest two frequencies than other pilots in Phase II, indicating that the pilot noticed the reduced phase margin due to the applied time delay and tried to cope with it, both in magnitude and phase content.

To compare differences in pilot control adaptations between simulators, the following sample figure is plotted, Figure 13.

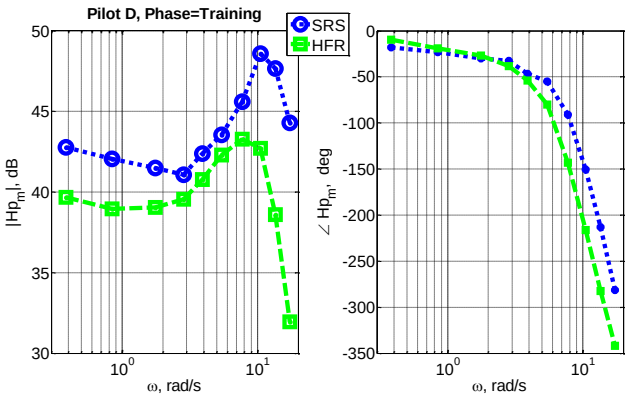

(a)

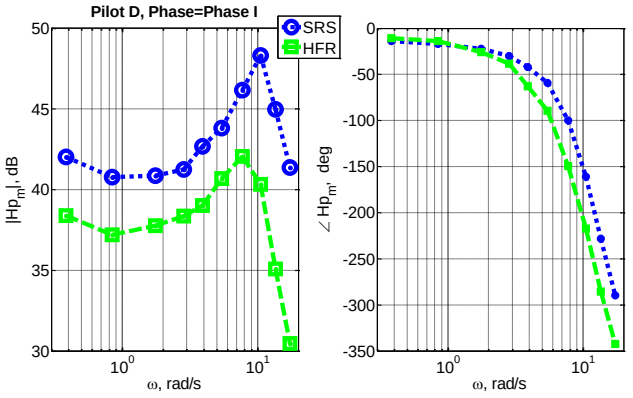

(b)

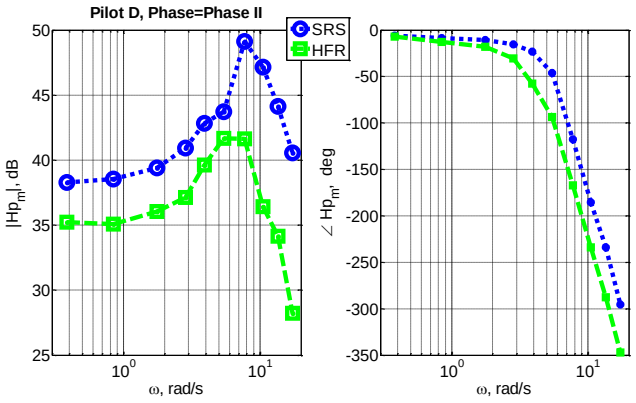

(c)

Figure 13. *Measured frequency responses of pilot D in both simulators for training (a), Phase I (b) and Phase II (c) of the task.*

Regardless of the task phase, Figure 13 shows that the offset between pilot magnitudes due to simulator differences (including physical differences of indicators, control inceptors, seating postures, etc.) and experimental differences (different experiment dates, pilot state of mind, more training, fatigue state, etc.). Consistent magnitude response and phase margin reduction are observed for Pilot D in HFR during all phases of the task. It may be a result of the introduction of greater lead compensation in SRS.

4.2 RPC Detection

Considering the definition for RPC presented in Section 1, detection in measured data, and concluding on the existence of RPC is a hard decision to make. In RPC events, the pilots, who are able to recognize the occurrence of a RPC event, simply back off after a couple of cycles or force themselves to avoid excessive inputs. Yet RPC's continue to occur, the ARISTOTEL project in Europe is taking initiative to expose RPCs in simulator environments in various aspects of RPC (e.g. criteria, simulator and design guideline development, etc.). One area of interest is the detection of the RPC in quasi real-time performance and possible post-processing applications. TUD aims to combine some aspects of Handling Qualities (HQ) criteria from ADS-33 [21] to enhance the existing Real-Time Oscillation VERifier (ROVER) [21], and UoL intends to make use of the newly conceived Phase Aggression Criteria [33].

This identification analysis used ROVER to determine the existing "possible" RPC's

Briefly, ROVER checks for peaks in excess of user-defined thresholds of stick activity, body rates, frequency of the input and the corresponding phase difference. Then, it provides ROVER 'flags', defining a ROVER score (number of individual flags at one time). Four flags (all activated) denote detection of PIO (the oscillatory RPC).

Threshold values used in ROVER for this identification experiment test are listed in Table 3. More information about ROVER can be found in references [31,32, 33].

Threshold name	*Value*	*Unit*
Stick amplitude	2.5	deg
Roll rate amplitude	18	deg/s
Frequency	1-8	rad/s
Phase delay	75	deg
Δstick extreme	0.2	deg
Δtime stick extreme	0.3	sec
Δroll rate extreme	1.2	deg/s
Δtime roll rate extreme	0.3	sec

Table 3: *Threshold values for ROVER*

It was assumed that the Phase II portion of each identification run (after 91.82 seconds) contained "possible" RPC events. An example of ROVER output is shown in Figure 14, displaying a clear increase in the total ROVER score following transition from Phase I to Phase II (an indication

of RPC proneness).

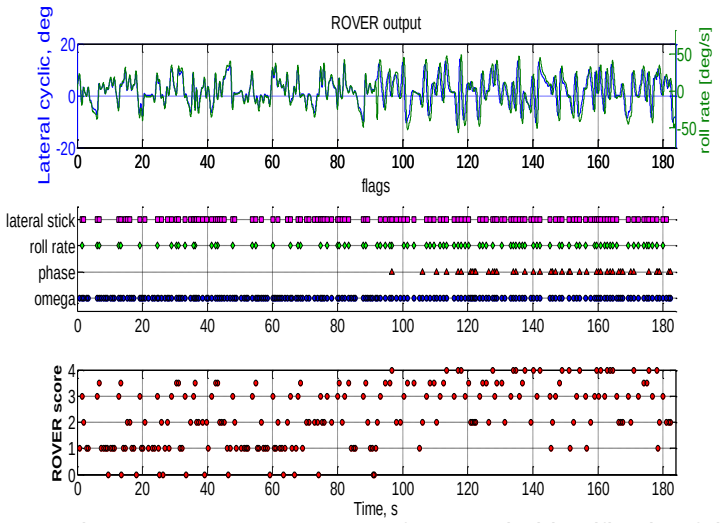

Figure 14. *ROVER output of a sample identification full run.*

Figure 14 displays the first occurrence of a ROVER score =4 immediately after transition to Phase II. The score is particularly influenced by phase flags resulting from the applied time delay (as would be expected). ROVER scores of all identification full runs for all pilots show similar trends; increased ROVER warnings and occurrences of "*ROVER detected"* PIO's in Phase II.

Hence, claiming that Phase II could lead to RPCs was confirmed with ROVER. Thus, any pilot model describing Phase II has a high chance of describing the "pilot model" during RPCs.

4.3 Pilot Model Structure Determination

The MLE and the second step of FC identification require a pilot model to describe the response of the pilot during the experiment. As for an initial prediction of the pilot model, the control element, (essentially an integrator up to ~10rad/s) requires gain compensation till the break frequency and a lead at the break frequency of the controlled element. This is in accordance with McRuer's Crossover model judgements; open loop PVS will have -20db/decade slope at the break frequency at which the 0 db magnitude defines the crossover frequency. After the first additional correction term for low frequency phase lag ($e^{-\alpha j\omega t}$)[1], McRuer's proposed a lead/lag compensation to capture the pilot low frequency lag in the Precision Model. The latter is thought to provide a better description of the pilot when considering the magnitude drop at low frequencies in measurement data (see Figure 12) and not only the low frequency phase lag.

The correction for low frequency is essential in this study because all pilots show the same low frequency lag adaptations. This is especially true for the lowest two frequencies of the disturbance signal (see Figure 12).

One reason for the existence of the low frequency magnitude cliff could be the long duration of the maximum left or right lateral stick input, which might end up as a low frequency response in the frequency domain analysis. However, the data were checked for the signature of such long durations of cyclic inputs at maximum deflections and no noticeable occurrences were observed.

Both identification techniques used the adapted precision pilot model as shown in Figure 15.

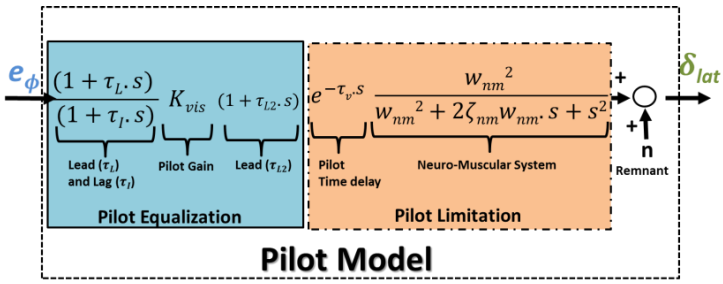

Figure 15. *Proposed pilot model, describing the pilot model block in* Figure 1, *with the adapted precision model Eq.* (6*), and the nonlinear pilot response; remnant (n).*

Figure 15 includes the pilot equalization for lead/lag at low frequency$(1+T_Ls/1+T_Is)$, pilot visual gain K_{vis}, lead $(1+T_{L2}s)$ for high frequency compensation of controlled element break frequency. The pilot limitation segment of the pilot model consists of pilot time delay (τ_v) and second order neuromuscular dynamics[16] adaptation with natural frequency (ω_{nm}) and damping (ζ_{nm}). Finally pilot remnant (n) was shown to reflect nonlinearities in pilot response arising from several sources [1]. Identification efforts in this paper do not include any remnant noise model, and it is assumed that there is no significant noise in the data, which was also shown in Figure 9–b (even in high frequencies the enriched frequency contains high signal to noise ratio).

4.4 Pilot performance and control activity

Two scales were used to assess the task performance and the control activity: RMS of displayed error (e_ϕ) and pilot control (δ_{lat}) respectively, shown in equations 7 and 8,

7) $RMSe = \sqrt{\frac{1}{N}\sum_{i=1}^{N} e_{\phi_i}^2}$

8) $RMSu = \sqrt{\frac{1}{N}\sum_{i=1}^{N} {\delta_{lat}}_i^2}$

For the remainder of the paper, the comparative figures are plotted per task, per pilot and per simulator. It must be noted that the main emphasis of this study was to compare the pilot adaptation between task phases, and to observe each pilots variance per task phase. The comparison between simulators is provided mainly to check the "trend of the pilot adaptation" consistency, not the absolute magnitudes. Therefore, scales of figures are adjusted by judging on deviation of std bars of the individual parameter figure, for each simulator.

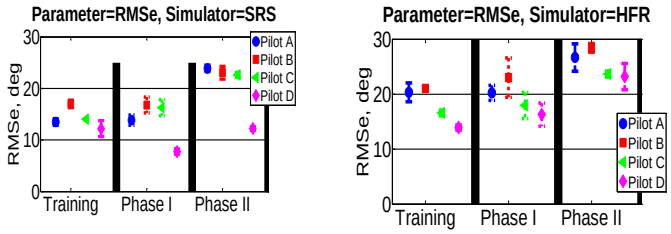

Figure 16. *RMS of perceived error mean and standard deviations per pilot, per task phase and per simulator.*

Figure 16 shows the RMS of displayed error of roll angle, which should be minimized by the pilot; the lower the value, the greater the performance. It is observed that in both SRS and HFR, pilots show similar performance for both training and Phase I, whereas lower performance (higher RMS) for Phase II. This was expected since the time delayed cyclic control in such a disturbance rejection task can easily lead to difficulty in capturing zero trim bank angle. The variance per pilot (the vertical std bars) was considered small for each task phase, with slightly more deviation in Phase II.

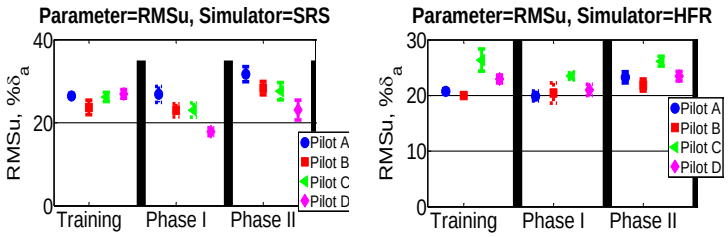

Figure 17. *RMS of deviation of pilot control deviation mean and standard deviations per pilot, per task phase and per simulator.*

Figure 17 shows the pilot control activity per phase per simulator. Regardless of variations between pilots, they all increased their control activity when experiencing the time delayed phase, Phase II.

To sum up, irrespective of simulator, all pilots had lower performance and higher control activity when experiencing a possible RPC scenario. Considering the degraded handling qualities of the controlled element, this was expected to be the case.

4.5 Pilot Model Fit

Since the low frequency magnitude drop and negative phase is apparent for all pilots in all simulators in this experiment set, a need for the low frequency fit was proposed, as performed by McRuer in Ref. [20]. This correction term in the present measurement data (lead/lag) requires a setting point for gain and a lag term that fits the first two lowest frequency data to have the negative slope in the magnitude plane and a negative starting phase value for the phase plane. As an example without lead, this pair of gain and lag terms are represented in a non-scaled descriptive plot, Figure 18, which resembles the observed actual low frequency responses of pilots in Figure 12.

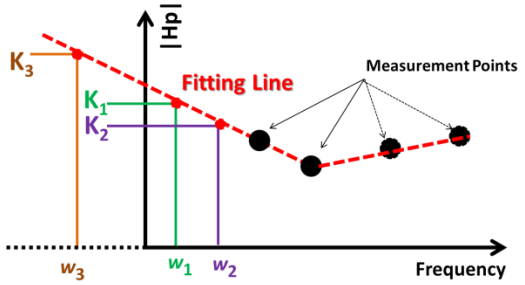

Figure 18. *Descriptive plot of pilot gain and lag frequency pairs that satisfies the fitting condition for low frequency lag of a representative measurement data in magnitude plane.*

In Figure 18, the red dashed fitting line represents the modelling line that allows a fit to the first two lowest frequency contents of the measurement data. The pilot visual gain and lag coupled pairs that can achieve the model fit are presented as $[K_1,w_1]$, $[K_2,w_2]$ and $[K_2,w_3]$. These three pairs successfully fit the model but $[K_1,w_1]$, $[K_2,w_2]$ may lead to a reasonable pilot gain and lag combination, whereas $[K_2,w_3]$ may lead to unachievable pilot gain and/or phase frequency. For the FC identification, the boundaries of the parameter optimisation allow a limit for parameters but still a forced result may end up with a "tweaked" parameter pool. On the other hand, MLE identification is not bounded. Therefore, the identification procedure may output extreme values of parameters but with a better fit. Therefore, a better time domain model fit but unrealistic parameter pool may appear in the MLE results, even though the initial parameter set of MLE is provided by the result of FC identification. This unrealistic parameter situation also appears in over-parameterised models when using time domain identification techniques [20]. The remedy to this situation could be including even lower frequencies in the disturbance function and omitting the lowest frequency, using the value as a manual tuning point for the identification. However, this solution also leads to an extended measurement time, which would lower the pilot concentration on the task. Sophisticated optimisation tools (e.g.

enhanced with Genetic Algorithms) to handle similar phenomena but in this paper, only the results of bare FC identification and Gauss-Newton gradient aided MLE are presented. They include those extreme values as well in parameter plots to point out the occurrences of such cases.

Another issue when using frequency and time domain identification methods in a comparative sense is the definition of cost function that must be in the domain to which the technique belongs. A good frequency fit parameter set may end up with a poor time domain fit, and vice-versa. Since MLE used in this study starts with the results of FC, several data proposed a better time domain fit but showed worse frequency fit. Likewise, a good frequency fit of FC sometimes showed low Variance Accounted For (VAF) values and mismatch in the time domain especially towards the end of the measurement time when the low frequency caused an offset in the time trace of the model fit.

Hence, extra care should be taken when interpreting the results with describing model fits with "good" and "bad". A good fit for both identification methods is considered the most desirable model.

4.5.1 FC Identification Pilot Model Fit

The proposed pilot model transfer function, shown in Figure 15, was embedded in the frequency domain and pilot model fitting was processed by minimizing the frequency domain error between the measurement data and the resultant pilot response, as described in Section 2.3.1.

VAF is a time domain measure of pilot model fit success and provides the information about how much of the time domain response is captured by the proposed model with the corresponding parameter set. The formulation of VAF used in this study is presented in Eq. (9);

$$VAF = \left(1 - \frac{\sum_{i=1}^{N} |\delta_{lat(i)} - \delta_{lat\_sim(i)}|^2}{\sum_{i=1}^{N} \delta_{lat(i)}^2}\right) \times 100\% \quad (9)$$

where δ_{lat_sim} is the pilot model simulated control input and N is the number of measurement points.

Thus, the higher the VAF, the better the model fit. The perfect fit is defined as 100%, all possible lower fits indicate the mismatched model structure, nonlinearities or noise included in the real measurement, which are not covered by the proposed LTI models. In the broad sense, the remaining VAF in this content can be judged as the remnant, pilot nonlinearities which have not been modelled. Besides, good VAF values do not guarantee the correct model structure, since unrealistic high order models may fit better but cannot explain the control strategy in the real application or may include parameters unachievable for a pilot [35]. Nevertheless, VAF values of the pilot model are presented in Figure 19. Note that the FC model is a frequency model, and VAF is a time domain measure. To obtain VAF values for the proposed FC pilot model fit, frequency domain representation was converted into the time domain using 5th order Padé approximation for time delays.

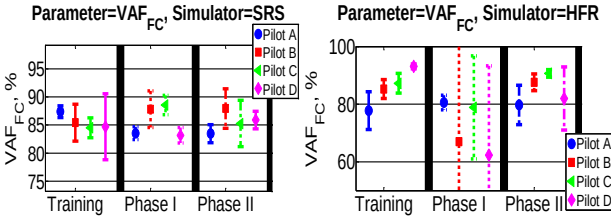

Figure 19. *VAF mean and standard deviations per pilot, per phase and per simulator.*

Results displayed in Figure 19 are considered to show good scores, with VAF values around 85-87% for SRS and similar for the HFR. This is with exception to Phase I for Pilot B and Pilot D in HFR, probably due to the aforementioned fitting issues such that even one extreme parameter value would induce high variance in the standard deviation of the data mean, clearly seen in Phase II portion of the HFR VAF results of Pilot B and Pilot D.

These VAF values indicate (but do not guarantee) that the FC model fit for all pilots in both simulators and all task phases is sufficient to represent the pilot control behaviour. The following figure shows a sample FC model fit with corresponding VAF value.

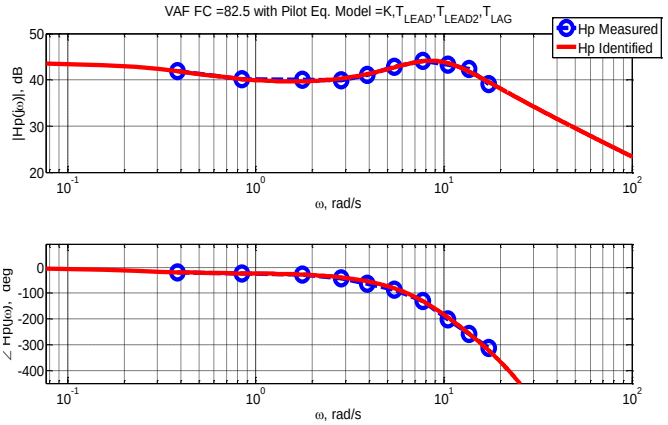

Figure 20. *FC pilot model fit to a sample measured identification data. VAF= 82.5% with the precision pilot model.*

Figure 20 shows a good frequency fit, with a close match of low frequency lag and high frequency neuromuscular response. Furthermore, corresponding VAF value (82.5%)

also indicates that this frequency fit also has a good time domain capture of pilot control to perceived roll angle error.

The following subsections describe the parameter variances of the proposed pilot model in further detail.

4.5.1.1 Pilot visual gain, K

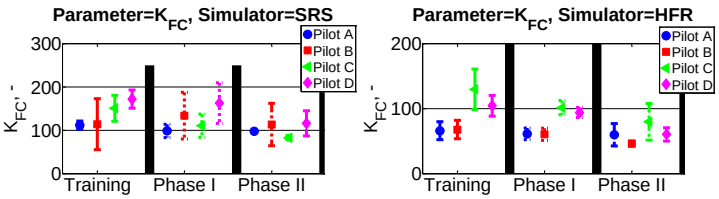

Figure 21. *Pilot gain mean and standard deviations per pilot, per phase and per simulator. Units of pilot visual gain is (%cyclic)/rad*

Figure 21 displays pilot visual gain distributions, showing that pilots lowered their visual gain from training and Phase I to Phase II, in both simulators. Pilots show better transfer of training to Phase I in HFR, likely due to the fact that they had already been introduced to the task and practiced in SRS earlier.

4.5.1.2 Lead time constant, T_{L1}

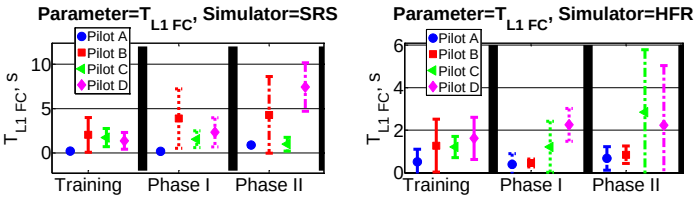

Figure 22. *Pilot lead constant (TL1) mean and standard deviations per pilot, per phase and per simulator.*

Figure 22 shows that Pilot A had almost the same lead constant throughout the identification experiment in all simulators and all phases. However, Pilot B, for example, showed a fluctuating trend in different simulators. Besides, as a general trend, pilots increased their lead time constants from training to the Phase I, then to the Phase II. This trend was more pronounced in SRS experiments.

4.5.1.3 Lag time constant, T_l

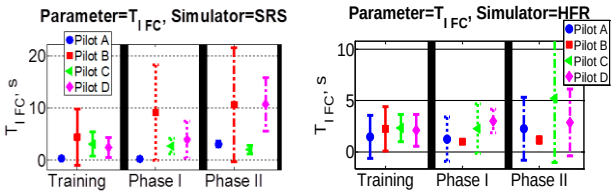

Figure 23. *Pilot lag constant (T_l) mean and standard deviations per pilot, per phase and per simulator.*

Figure 23 shows that, particularly in SRS, there is a clear increase in pilot lag from training and Phase I to Phase II. Theoretically, also presented in Figure 11-b, translating from Phase I to Phase II requires lower gain and lower lag frequency when considering the frequency content of the measurement data. In HFR, with the exception of Pilot B, all pilots showed the same trend with increasing variances.

4.5.1.4 Lead time constant, T_{L2}

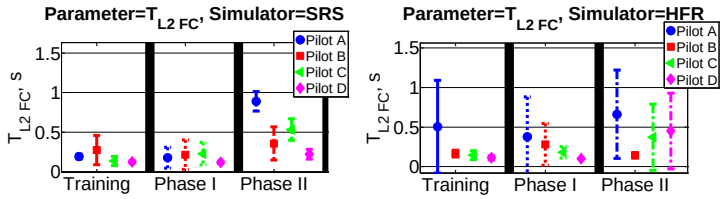

Figure 24. *Pilot lead constant (T_{L2}) mean and standard deviations per pilot, per phase and per simulator.*

Figure 24 presents the lead time constant deviation for pilots in different simulators, and various task phases. The 2nd lead time constant was introduced in the proposed pilot model to compensate the change of controlled element break frequency. Hence, it was expected to have consistent values (depending on the neuromuscular activation which seldom had peaks around the break frequency). Particularly in SRS, this expectation was satisfied ($T_{L2} \cong 1/\omega_b$). In HFR, the general tendency was captured, but with a higher variance in Phase II.

4.5.1.5 Pilot Limitations, $\omega_{nm}, \zeta_{nm}, \tau_v$

The pilot limitations block in the proposed pilot model (Figure 15) depends on the pilot's physiological properties, control inceptor dynamics and his response time to the perceived trigger. It was expected to be constant per pilot regardless of the phase of the task, but vary with different simulators.

The following Figure shows the three pilot limitation parameters per pilot, per phase and per simulator.

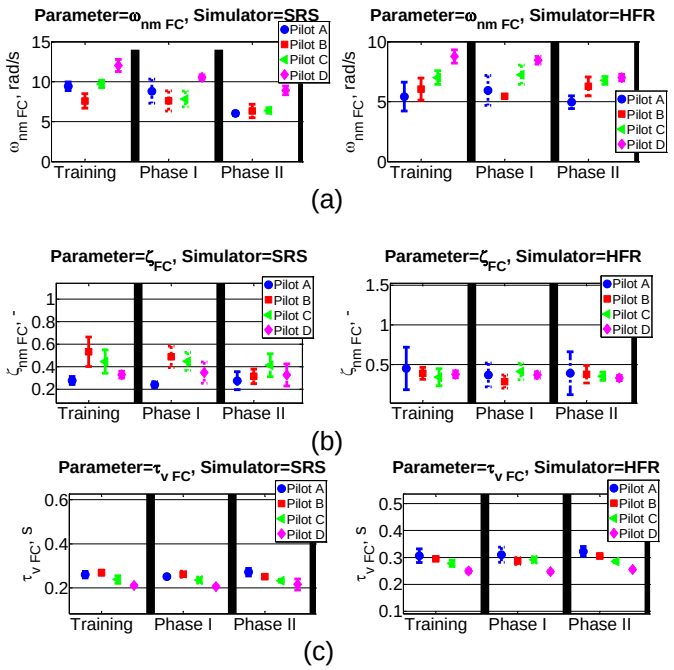

Figure 25. a.)*Pilot neuromuscular system frequency (ω_{nm}), b.)Pilot neuromuscular system damping (ζ_{nm}), c.)Pilot time delay (τ_v) ; mean and standard deviations per pilot, per phase and per simulator.*

Figure 25 verifies the expectation of achieving the same pilot limitation characteristics per pilot in all task phases and simulators. Moreover, the differences in pilot limitations were revealed, e.g. Pilot B had lower natural neuromuscular natural frequencies and higher damping than Pilot D, regardless of compared simulator runs. All pilots were found to have close time delays, which indicate the time to achieve desired muscular activation.

This investigation leads to the conclusion that pilot limitation does not change in RPCs, but the active pilot control parameters (pilot equalisation) are subjected to change for various task phases and simulators.

4.5.1.6 Crossover Frequencies (ωc) and Phase Margins (Φ_M)

Another performance criterion is the PVS open loop crossover frequency and the corresponding phase margin that indicates the available phase angle until the instability (-180 degrees). A sample run is shown in Figure 26.

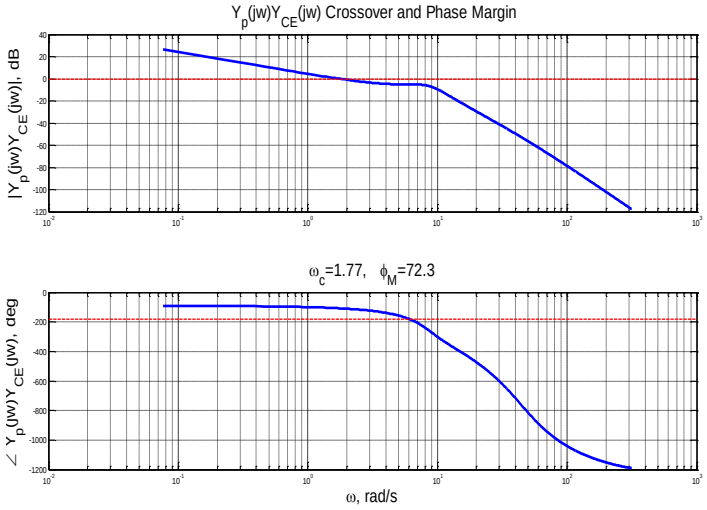

Figure 26. *A sample plot of crossover frequency (1.77 rad/s) and phase margin (72.3 degrees).*

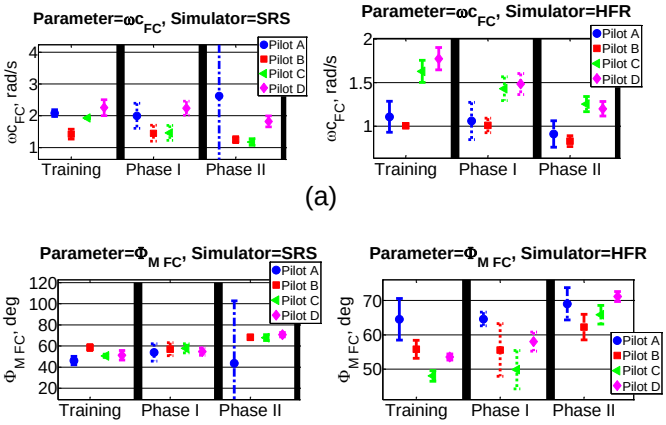

Figure 27. a.)*Pilot crossover frequencies (ωc), b.)Phase Margin (Φ_M); mean and standard deviations per pilot, per phase and per simulator.*

Figure 27 shows that overall crossover frequencies are noticeably low when compared to regular operational crossover frequencies. Keeping in mind that this experimental setup would introduce more difficult and intense pilot effort with the absence of regular operational feedback, e.g. motion and visual cues, pilots might experience difficulties in fulfilling the task requirements. This may have resulted in the observed low crossover frequencies.

<u>Possible reasons for low crossover frequencies:</u>

1. High power spectra at high frequencies

Rich high frequency content of the disturbance function may lead pilots to regress their crossover frequency to where they can have better control margin. This adaptation is called *Crossover Regression,* and several items in the literature have investigated the triggering conditions for crossover regression [1,36,37] and

its application to handling qualities assessment [38].

2. Lack of enough training sessions of the task

Identification experiments in both simulators were conducted within the daily simulator programs of the first RB test campaign of ARISTOTEL project. As the simulator trials included ADS-33[21] MTEs with highly aggressive and RPC benchmarking conditions, the identification tests were limited by time constraints, which resulted in only a short time for pilots to adapt themselves to the task and the controlled element responses. Even though training and Phase I sections showed good correlation among all pilots per simulator, approximately 25 minutes of one pilot experiment (total training and full length runs) is thought to be not enough for human operators to achieve well trained high crossover frequencies with high level of linear adaptation.

3. Nature of the compensatory tracking simulation

In Ref. [34], Mitchell reported the usage of US Air Force Large Amplitude Multimode Research Simulator (LAMARS) to investigate the extraction of pilot models from mimicked SOS and discrete tracking tasks, which were actually flown in test flights of HAVE LIMITS[41] project. Although the vehicle dynamics, triggers and the whole experiment setup was different than the experiment set in this paper, the crossover frequencies were experienced around 1.4-1.7 rad/s for various configurations of aircraft. When compared to Figure 27 –a, it is observed that the obtained low crossover frequencies may be due to the nature of the SOS tracking task, which forces pilots into a more conservative state, leading to a compromise between task performance and stability of the PVS. Pilots might prefer to sacrifice performance to achieve safer stability response.

With regards to phase margin, it can be observed from Figure 27 –b that pilots increased their phase margins while translating from training and Phase I to Phase II.

4.5.2 MLE Identification Pilot Model Fit

A sample MLE result is shown in Figure 28.

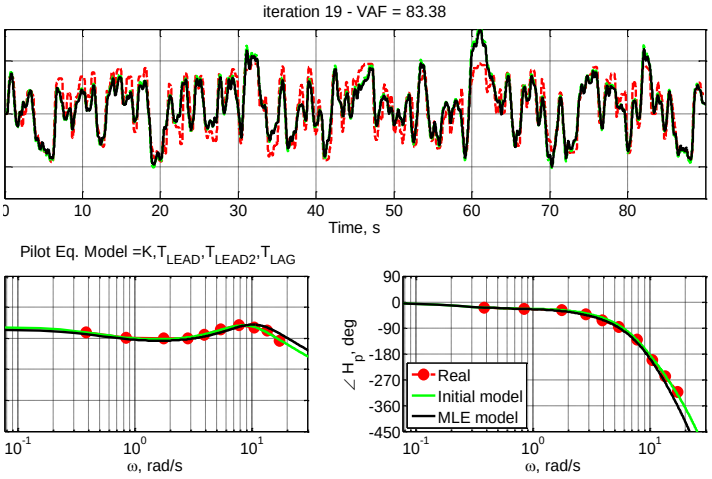

Figure 28. *A sample plot of MLE identification result, showing the actual measurement data, initial and final MLE model fit, with the corresponding iteration number and VAF.*

It is seen from Figure 28 that MLE aims to reduce the time domain error between the actual measurement data (red line) and the final model fit (black line), starting from the initial model (green line),which was provided from FC identification. An increase in VAF values, which refers to better time domain fit as well, was achieved with the cost of slight mismatch in frequency domain, especially at high frequencies. Overall VAF values are shown in Figure 29.

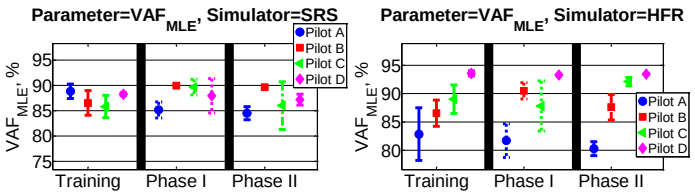

Figure 29. *VAF mean and standard deviations per pilot, per phase and per simulator.*

Figure 29. shows that VAF values of MLE are higher when compared to FC values. This is also due to the nature of MLE which tries to have better time domain fit, which can be interpreted as VAF as well.

4.5.2.1 Pilot visual gain, K

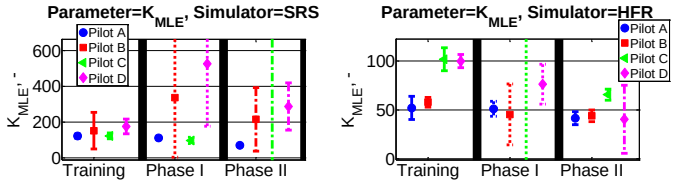

Figure 30. *Pilot gain mean and standard deviations per pilot, per phase and per simulator. Units of pilot visual gain is (%cyclic)/rad.*

Regardless of parameter overshoots, pilot gain distributions, plotted in Figure 30, show that pilots lowered their visual gain from Phase I to Phase II, in both simulators. MLE identification showed high variances in both Phase I and Phase II, which is an indication of parameter fitting to extreme values since MLE does not hold any parameter boundaries.

4.5.2.2 Lead time constant, T_{L1}

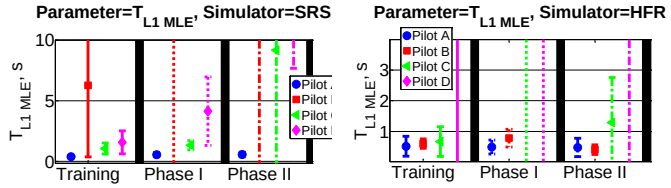

Figure 31. *Pilot lead constant (TL1) mean and standard deviations per pilot, per phase and per simulator.*

Figure 31 shows that MLE had several parameter fits which exceeded beyond human operator limits, but provided better time domain measurement fit. Like the HFR results of FC identification.
In Figure 31, pilots showed more or less consistent lead time in both simulators, according to MLE identification.

4.5.2.3 Lag time constant, T_l

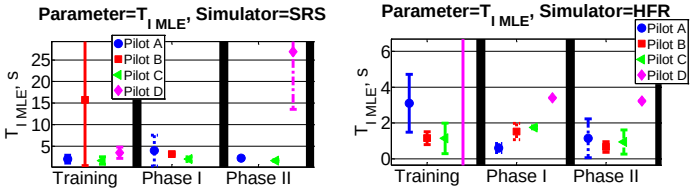

Figure 32. *Pilot lag time constant (T_l) mean and standard deviations per pilot, per phase and per simulator.*

Figure 32 shows approximately the same trend between Phase I and Phase II for MLE identification. Considering FC results, MLE could not show any significant deviation in lag time constant, except the extreme fitting for Pilot B and Pilot D in SRS.

4.5.2.4 Lead time constant, T_{L2}

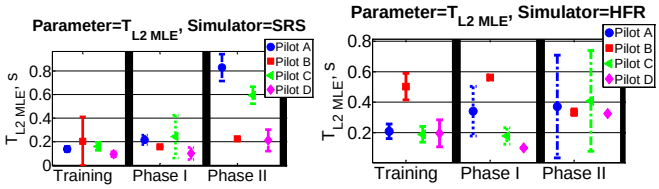

Figure 33. *Pilot lead time constant (T_{L2}) mean and standard deviations per pilot, per phase and per simulator.*

Figure 33 presents the lead time constant deviation for pilots in different simulators, and various task phases. Similar results were obtained when compared to FC identification,
Figure 24. Hence, the same interpretation of the controlled element break frequency capture is also valid for MLE identification results for the second lead time constant parameter.

4.5.2.5 Pilot Limitations, $\omega_{nm}, \zeta_{nm}, \tau_v$

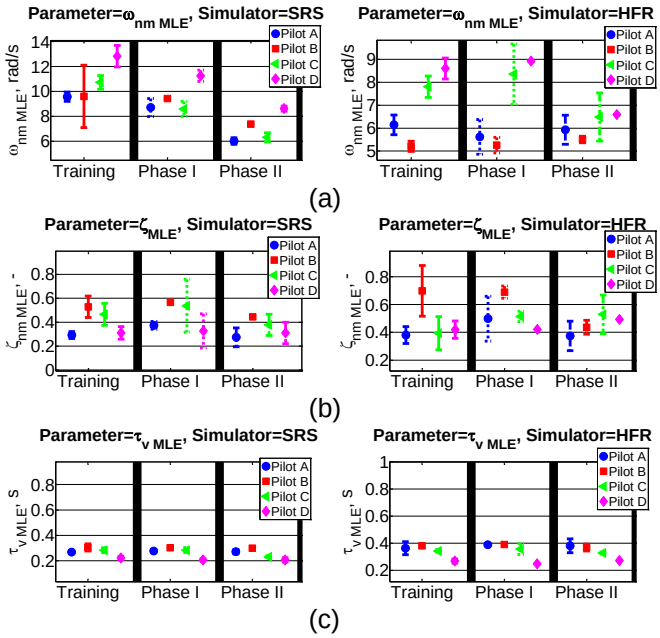

Figure 34. a.)*Pilot neuromuscular system frequency (ω_{nm}), b.)Pilot neuromuscular system damping (ζ_{nm}), c.)Pilot time delay (τ_v) ; mean and standard deviations per pilot, per phase and per simulator.*

Like FC identification results, MLE identification also showed that pilot limitations (Figure 34) are almost equal for various task phases and simulators.

The same conclusion can be drawn similar to FC identification: pilot limitation parameters are similar but pilot adaptation mainly occurs for pilot equalisation parameters, during possible RPC.

4.5.2.6 Crossover Frequencies (ωc) and Phase Margins (Φ_M)

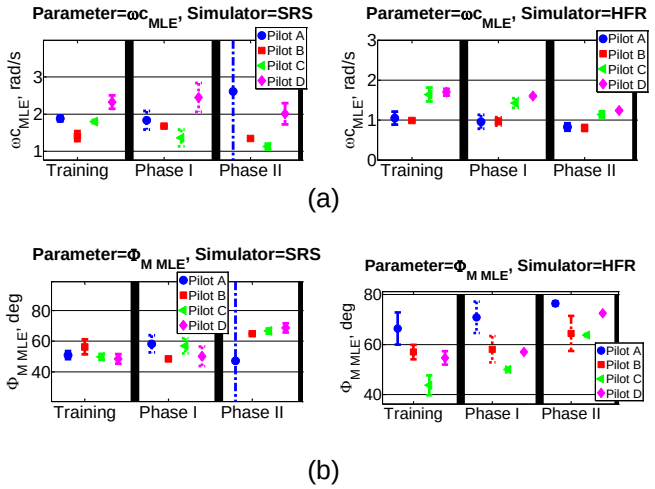

Figure 35. a.)*Pilot crossover frequencies (ωc), b.)Phase Margin (Φ_M); mean and standard deviations per pilot, per phase and per simulator.*

Figure 35 indicates that MLE identification method resulted in slightly higher crossover frequencies, with phase margin similar to that determined during FC identification. Like FC, MLE showed that pilots had a small increase in their phase margins from training and Phase I to Phase II. This behaviour displays the tendency of pilots to have better stability by increasing phase margin during a possible RPC case.

5. CONCLUSIONS AND RECOMMENDATIONS

A set of pilot identification experiments was conducted in two flight simulators with four helicopter pilots. The task was a roll disturbance-rejection single loop compensatory manual control task, with a controlled element representative of the Bo105 roll response to pilot control. The scope of the experiment was to detect pilot adaptation to an online applied time delay, designed to cause RPC tendencies by using frequency and time domain identification techniques, FC and MLE respectively. Key conclusions of this investigation are shown below;

- Measurement data showed that all pilots changed their response to perceived roll error in the compensatory task from no- RPC partition (training and Phase I) to possible RPC partition (Phase II). This pilot adaptation was consistent irrespective of simulator.
- To determine the presence of RPC in the Phase II partition of the run, ROVER was applied, which displayed a clear increase in PIO tendency, though the activation of warning flags. Therefore, it was assumed that Phase II was a suitable task phase to be representative of “possible” RPC events.
- By adjusting McRuer’s Precision Model with low frequency lag, a pilot model was proposed and used in both identification methods used to fit the measured data.
- It was observed that pilots reduced their visual gains during possible RPC events, especially at low frequencies.
- Pilots tended to increase their low frequency lead, to overcome the phase reduction caused by the additional time delay in the control path.
- Pilots kept their own limitation parameters almost constant, namely neuromuscular dynamics and internal time delays, throughout all phases of the experiments in each simulator. Moreover, pilots show different limitations among each other in each simulator.
- Frequency domain FC identification showed good frequency pilot model fit, with sufficient VAF scores. However, unbounded MLE identification seldom reached unrealistic parameter values but achieved better VAF scores.
- Due to the high disturbance power at high frequencies and the lack of training prior to task completion, pilots showed lower crossover frequencies and higher phase margins than initially expected. In addition, during possible RPCs, pilots further tried to increase the phase margins. This shows that pilots tended to sacrifice task performance but in return tried to achieve better stability to counteract the perceived RPC.

Recommendations

- High frequency content of the disturbance signal was sufficiently high that it led to “difficult” task performance with low crossover frequencies. Since the main pilot adaptation is observed in the low frequency range (0.3 to 5 rad/s), it is recommended that lower power is used for high frequencies within the disturbance forcing function. The authors recommend 40-60dB difference should be sufficient. However, this should be tested prior to further investigation.
- Due to limited time during the ARISTOTEL RB test campaign, the familiarization and training to the task and controlled element was probably not long enough to achieve linear pilot control behaviour. Thus, the validity of LTI identification methods is questionable. However, the comparison between training and Phase I showed similar trends. To increase the signal to noise ratio it is recommended to have more repetitions per measurement point.

- One fundamental setting in such a basic experiment is the control device specifications. Because, it defines the magnitude of pilot input to achieve the task performance, and various dynamic properties of the control inceptors are subjected to change between simulators. Although it was aimed to match the cyclic settings among SRS and HFR, it recommended to match further detailed specifications; mass of the inceptor, force gradients, etc.
- A statistical analysis, e.g. ANOVA[42], would show cross dependency of parameters and would provide more information about variances and effects on the results.

- The low frequency adaptation terms lead, especially unbounded MLE, to reach extreme values which are not achievable by human pilots. It is proposed that using a new equalisation parameter which couples gain and lag time constant together would aid to reduce flexibility in the gradient based Gauss-Newton optimization of MLE.Hence, the equalization term in the pilot model may be rearranged :

(10) $Pilot\ Equalization = H^*(\tau_{L1}s + 1)(\tau_{L2}s + 1)$

where,

(11) $H^* = K(1/s)$

By this parameter adaptation, it may be possible to couple the gain and the lag, and the reduced number of parameters would help optimizations to converge. On the other hand, interpretation of the new parameter, H^*, would be hard to conclude on results, because direct pilot parameters would be merged in this new one. Any value would be a total effect of unrealistic couples, but at least a set of combination would be available for better optimisation.

- During the experiment runs, pilots were focusing on a single source attitude indicator model on the screen, further concentrating on small bank errors. This visually intensive work caused a drop of attention during the full runs, which lasted approximately three minutes each. To maintain attention level and provide a performance rating, it would be beneficial to provide a performance score, e.g. RMS of error, to force pilots not to back-off and keep their motivation to increase their performance after each run.

Acknowledgements

This study was conducted within the ARISTOTEL project (Aircraft and Rotorcraft Pilot Couplings – Tools and Techniques for Alleviation and Detection, ACPO-GA-2010-266073) of 7th Framework Programme of European Commission. The author sincerely thanks to Daan Pool, Herman Damveld, Olaf Stroosma and Shafiek Suliman for their aid and effort in all stages of this experimental study.

REFERENCES

1. McRuer, D., Graham, D. , Krendel,. E., Reisener, W., "*Human Pilot Dynamics in Compensatory Systems*", Tech. Report: AFFDL-TR-65-15, Airforce Flight Dynamics Laboratory, Wright-Patterson Air Force Base, Ohio, July 1965
2. McRuer, D., et al., "*Aviation Safety and Pilot Control. Understanding and Preventing Unfavourable Pilot-Vehicle Interactions*", ASEB National Research Council, National Academy Press, Washington D.C., 1997.
3. Nieuwenhuizen, F. Beykirch K. A., Mulder M., Bülthoff, H.H. "*Identification of Pilot Control Behaviour in a Roll-Lateral Helicopter Hover Task*", Proceedings of the AIAA Modeling and Simulation Technologies Conference and Exhibit, Hilton Head (SC), No AIAA-2007-6799, Aug. 2007.
4. Schroeder, J.A.," *Helicopter Flight Simulation Motion Platform Requirements*", Tech. Rep. NASA/TP-1999-208766,NASA, July 1999.
5. Whalley, M. ,Howitt, J., "*Optimization of Partial Authority Flight Control Systems for Hover/Low-Speed Manoeuvring in Degraded Visual Environments*", Journal of the American Helicopter Society, Vol. 47,No. 2, April 2002, pp. 79-89.
6. Zaal M.T., Sweet B.T.*,"Estimation of Time-Varying Pilot Model Parameters*", AIAA Modeling and Simulation Technologies Conference, 8-11 Aug. 2011, Portland, Oregon.
7. Klyde D.H, Schulze P.C., Thompson P.M., Liang C.L., "*Use of Wavelet Scalograms to Characterize Rotorcraft Pilot-Vehicle System Interactions*", American Helicopter Society 66th Annual Forum, 11-13 May, 2010.
8. Hess R.A., "*A Preliminary Study of Human Pilot Dynamics in the Control of Time-Varying Systems*", AIAA 2011-6554, AIAA Modeling and Simulation Technologies Conference, 8-11 Aug. 2011, Portland, Oregon.
9. Pavel, M. D., Malecki,J., DangVu,B., et al. , "*Present and Future Trends in Rotorcraft Pilot Couplings (RPCs) - A Retrospective Survey of Recent Research Activities within the European Project ARISTOTEL*," European Rotorcraft Forum, ERF, Varese, Italy, 2011.
10. McRuer,D. T. , "*Pilot-Induced Oscillations and Human Dynamic Behavior*," NASA Contractor Report 4683,July 1995.
11. Pavel,M.D., Dang Vu,B., Gotz,J., Jump,M. and Dieterich,O. , "*Adverse Rotorcraft-Pilot Couplings - Prediction and Suppression of Rigid Body RPC Sketches from the Work of Garteur HC-AG16*," 34th European Rotorcraft Forum, RAeS European Rotorcraft Forum, Liverpool, UK, 2008.

12. Mitchell,D. G. and Klyde,D. H. , "*Identifying a PIO signature - New techniques applied to an old problem*," 2006 Atmospheric Flight Mechanics Conference, August 21, 2006 - August 24, American Institute of Aeronautics and Astronautics Inc, Keystone, CO, United states, 2006.
13. Walden,R. B. , "*A Retrospective Survey of Pilot-Structural Coupling Instabilities in Naval Rotorcraft*," American Helicopter Society 63rd Annual Forum, American Helicopter Society, 2007.
14. Stapleford, R. L., Peters, R. A., and Alex F.R., "*Experiments and Model for Pilot Dynamics with Visual and Motion Inputs*", *NASA CR-1325*, 1969.
15. Mulder, M. "*Cybernetics of Tunnel-in-the-sky Displays*", Doctoral dissertation, Faculty of Aerospace Engineering, Delft University of Technology, 1999.
16. Van Passen, M.M., "*Biophysics in Aircraft Control, A Model of the Neuromuscular System of Pilot's Arm*", Doctoral dissertation, Faculty of Aerospace Engineering, Delft University of Technology, 1994.
17. Vinje, E. W., Pitkin, E. T.," *Human Operator Dynamics for Aural Compensatory Tracking*", Seventh Annual Conference on Manual Control. NASA SP-281, Washington, D.C., 1972[31]Anon. , "The SIMONA Research Simulator," 2012.
18. Perfect,P., White,M., Padfield,G. D., Gubbels,A. W. and Berryman,A., "*Integrating Predicted and Perceived Fidelity for Flight Simulators*," European Rotorcraft Forum 2010, 2010.
19. MATLAB® documentation, section "toolbox - optimization - lsqnonlin", 2012.
20. Zaal, P.M.T., Pool, D.M., Chu Q.P., Van Paassen M. M., Mulder, M. and Mulder, J. A.,"*Modeling Human Multimodal Perception and Control Using Genetic Maximum Likelihood Estimation*", Journal of Guidance, Control, and Dynamics, Vol. 32, No. 4, 2009, pp. 1089-1099
21. Anon., "*Aeronautical Design Standard Performance Specification Handling Qualities Requirements for Military Rotorcraft*," United States Army Aviation and Missile Command Aviation Engineering Directorate, Redstone Arsenal, Alabama, 2000.
22. Breur, Sjoerd W., Pool, Daan M., van Paassen, Marinus M. and Mulder, Max, "*Effects of Displayed Error Scaling in Compensatory Roll-Axis Tracking Tasks*", AIAA-2010-8091, Proceedings of the AIAA Guidance, Navigation, and Control Conference, Toronto, Canada, 2010
23. Grant, P.R., and Schroeder, J. A.,"*Modeling Pilot Control Behaviour for Flight Simulator Design and Assessment*", AIAA Guidance, Navigation, and Control Conf., AIAA Paper 2010-835, Toronto, Aug. 2010
24. Stroosma,O., Van Paassen,M. M. and Mulder,M. , "*Using the SIMONA research simulator for human-machine interaction research*," AIAA Modeling and Simulation Technologies Conference and Exhibit, 2008.
25. Anon., "*Advanced Rotorcraft Technology Heliflight-R Technical Documentation*," Advanced Rotorcraft Technology, 2007
26. Padfield, G. D., "*Helicopter Flight Dynamics*", 2nd ed., Blackwell Science, Oxford, 2007
27. Mohammad, M.L., Alastair, K.C. "*Review of pilot modeling techniques*", 48th AIAA Aerospace Sciences Meeting, AIAA 2010-297, 4-7 January 2010, Orlando, US
28. Drop, Frank M.,"*Feed Forward Behavior in Manual Control Tasks With Predictable Target Signals*", MSc Thesis, Delft University of Technology, Faculty of Aerospace Engineering, May. 2011.
29. Mark Tischler M and Remple R.," *Aircraft and Rotorcraft System Identification*", Published by AIAA Education Series, ISBN 978-1-60086-007-2 , 2006
30. Van der Pols, R.H. ,"*Multimodal Pilot Model Identification on the Desdemona Simulator*", MSc. Thesis, Delft University of Technology, Faculty of Aerospace Engineering, Feb. 2012
31. Mitchell, D.G., A.J. Arencibia and S. Munoz: "*Real-Time Detection of Pilot-Induced Oscillations*", AIAA-04-4700 Atmospheric Flight mechanics Conference, Providence, RI, 16-19 August 2004.
32. Suliman M.T.S., Yilmaz D., Pavel, M.D., "*Harmonizing The Realtime Oscillation Verifier (Rover) With Handling Qualities Assessment For Enhanced Rotorcraft Pilot Couplings Detection*", 38th European Rotorcraft Forum, ERF, Amsterdam, The Netherlands, September 2012
33. Jones, M., Jump, M., Lu, L., Yilmaz, D., Pavel M. D.: "*Using the Phase-Agression Criterion to Identify Rotorcraft Pilot Coupling Events*", 38th European Rotorcraft Forum, ERF, Amsterdam, The Netherlands, September 2012
34. Mitchell, D.G., *"Identifying the Pilot in Pilot Induced Oscillations*", AIAA Atmospheric Flight Mechanics Conference, AIAA-2000-3985, Denver ,14-17 Aug. 2000
35. Pool, D. M. , Zaal, P. M. T., Damveld, H. J.,van Paassen, M. M.,van der Vaart, J. C. and Mulder, M.," *Modeling Wide-Frequency-Range Pilot Equalization for Control of Aircraft Pitch Dynamics*", Journal of Guidance, Control, and Dynamics, Vol.34 Num.5, p 1529-1542, Sept.-Oct. 2011
36. Elkind, J. I., "*Characteristics of Simple Manual Control Systems*" ,Ph. D. Thesis, Lincoln Lab., Massachusetts Inst. of Technology , Cambridge, MA, 1956
37. G.C Beerens, H. J. Damveld, M. Mulder, M. M. van Passen and J.C. "*Investigation Into Crossover Regression in Compensatory Manual Tracking Tasks*", Journal of Guidance , Control, and Dynamics, Vol. 32, No .5, Sept.-Oct. 2009
38. Damveld, Herman J., "*A Cybernetic Approach to Assess the Longitudinal Handling Qualities of Aeroelastic Aircraft*", PH. D. Thesis, Delft University of Technology, Faculty of Aerospace Engineering, May 2009
39. Mitchell, D.G. and B.K. Stadler, "*Simulation Investigation of Category I and II PIO*", AIAA Atmospheric Flight Mechanics Conference, AIAA-99-403, Portland, Aug. 1999

40. Bjorkman, E.A., Capt., USAF, et al, "*NT-33 Pilot Induced Oscillations Prediction Evaluation*", USAFTPS-TR-85B-S4, June 1986.
41. Kish, B.A., et al., "*A Limited Flight Test Investigation of Pilot-Induced Oscillation due to Elevator Rate Limiting*", AFFTC-TR-97-12, June 1997.
42. Freedman, D. A.,"*Statistical Models: Theory and Practice"*, Cambridge University Press. ISBN 978-0-521-67105-7., 2005
43. Zaal, P. M. T., Pool, D. M., De Bruin, J., Mulder, M., and Van Paassen, M. M., *"Use of Pitch and Heave Motion Cues in a Pitch Control Task*,"Journal of Guidance, Control, and Dynamics, Vol. 32, No. 2, 2009,pp. 366–377.
44. Zaal, P. M. T., Mulder, M., Van Paassen, M. M., and Mulder, J. A.,"*Maximum Likelihood Estimation of Multi-Modal Pilot Control Behavior in a Target-Following Task*," Proceedings of the IEEE Conference on Systems, Man, & Cybernetics (IEEE—SMC),New York, Oct. 2008, pp. 1085–1090.